

Thermal Elastohydrodynamic Lubrication of Line Contact Rough Surfaces Using Flow Factor Method

Hasim Khan and Prawal Sinha

Department of Mathematics and Statistics,
Indian Institute of Technology Kanpur,
Kanpur-208016, India
hashim@iitk.ac.in, prawal@iitk.ac.in

Abstract

A complete solution of a thermal elastohydrodynamic lubrication (EHL) of rolling/sliding rough surfaces is obtained. The modified average Reynolds equation, elasticity equation and energy equations are solved simultaneously using a modified Houpert and Hamrock fast approach. The dimensionless pressure, film thickness, mean film temperature and surface temperature distributions are obtained for various values of surface roughness parameters. The results are compared with that of isothermal rough EHL and thermal smooth EHL. The inclusion of thermal effect has significantly influenced the bearing characteristic for rough EHL problem.

Keywords: Infinite line contacts, Thermal-EHL, Surface Roughness.

1 Introduction

Surface roughness plays an important role in deciding the behavior of lubricated machine elements such as gears, cams, roller bearings and ball bearings operating under heavily loaded conditions. Under such conditions, very high pressures are generated near the asperity contact regions. This reduces the film thicknesses and gives rise to large frictional forces resulting in an increase in film and surface temperatures.

The study of surface roughness in hydrodynamic lubrication analysis was pioneered by Citron [1] with deterministic surface roughness models having sinusoidal or saw-tooth distribution. Christensen and Tonder [2] developed the stochastic Reynolds equation for transverse and longitudinal surface roughness. Cheng and Dyson [3] obtained a complete solution for the inlet half of line-contact EHL by

using the Stochastic Reynolds equation. Patir and Cheng [4] introduced a new method of deriving the average Reynolds equation through flow simulation which incorporates the effects of surface roughness on EHL of line contacts. Majumdar and Hamrock [5] and Prakash and Czichos [6] considered the flow model proposed by Patir and Cheng [4] and used pressure-compliance relationship derived by Greenwood and Tripp [7] to obtain a complete solution of incompressible EHL of rolling contact of rough surfaces having identical structure. Wang and Lin [8] employed the average Reynolds equation developed by Patir and Cheng [4] through flow simulation to obtain the hydrodynamic pressure in EHL of infinite line contacts with compressibility and sliding effects.

The solution of thermal EHL of rolling/sliding line contacts incorporating deterministic surface roughness was obtained by many researchers such as Sadeghi and Sui [9], Kumar et al. [10], Kumar et al. [11] and Almqvist and Larsson [12]. An attempt to analyze the thermal EHL of rough surfaces using stochastic approach has not appeared in the literature. Hence, this study may be considered as a first attempt towards a complete solution of randomly rough EHL including thermal effects.

In the present study, the elasticity equation, energy equations and modified average Reynolds equation [8] incorporating the surface roughness through flow factors and average film gap with Gaussian distribution of asperity height, are solved simultaneously to obtain a complete numerical solution of thermal EHL of rolling/sliding rough surfaces.

2 Mathematical Model

The average Reynolds equation for fluid-film lubrication of rough surfaces employed by Wang and Lin [8] to calculate the hydrodynamic pressure in EHL line contact can be expressed as :

$$\frac{\partial}{\partial x} \left(\phi_x \frac{\bar{\rho} h^3}{12\bar{\eta}} \frac{dp}{dx} \right) = \frac{(u_a + u_b)}{2} \frac{\partial(\bar{\rho}\bar{h}_T)}{\partial x} + \frac{(u_a - u_b)}{2} \bar{\sigma} \frac{\partial(\bar{\rho}\phi_s)}{\partial x} \quad (1)$$

Assuming the same surface structure and the same rms roughness of surfaces, under such circumstances the shear flow factor ϕ_s vanishes and the Reynolds equation for thermal and steady state conditions can be written as :

$$\frac{\partial}{\partial x} \left(\phi_x \frac{\bar{\rho} h^3}{12\bar{\eta}} \frac{dp}{dx} \right) = u_m \frac{\partial(\bar{\rho}\bar{h}_T)}{\partial x}, \quad \text{where, } u_m = \frac{(u_a + u_b)}{2} \quad (2)$$

Using the following dimensionless quantities :

$$X = \frac{x}{b}, P = \frac{p}{p_H}, H = \frac{hR_x}{b^2}, \eta = \frac{\bar{\eta}}{\eta_0}, \rho = \frac{\bar{\rho}}{\rho_0}, P_c = \frac{p_c}{p_H}, \bar{H}_T = \frac{\bar{h}_T R_x}{b^2}$$

$$\sigma = \frac{\bar{\sigma} R_x}{b^2}, W = \frac{w}{ER_x}, W_t = \frac{w_t}{ER_x}, H_0 = \frac{h_0 R_x}{b^2}, U = \frac{\eta_0 u_m}{ER_x}, G = \alpha E \quad (3)$$

The dimensionless Reynolds equation can be rewritten as:

$$\frac{\partial}{\partial X} \left(\phi_x \frac{\rho H^3}{\eta} \frac{dP}{dX} \right) - \lambda \frac{\partial}{\partial X} (\rho \bar{H}_T) = 0, \quad \text{where, } \lambda = \frac{12\eta_0 u_m R_x^2}{b^3 p_H} \quad (4)$$

ρ and η are functions of pressure and mean film temperature. The boundary conditions for equation (4) are :

$P = 0$ at $X = X_{in}$ and $P = dP/dX = 0$ at $X = X_{out}$.

The average film-gap \bar{h}_T shown in figure 1, is the expected value of $(h + \delta)$ as follows-

$$\bar{h}_T = \int_{-h}^{\infty} (h + \delta) f(\delta) d\delta \quad (5)$$

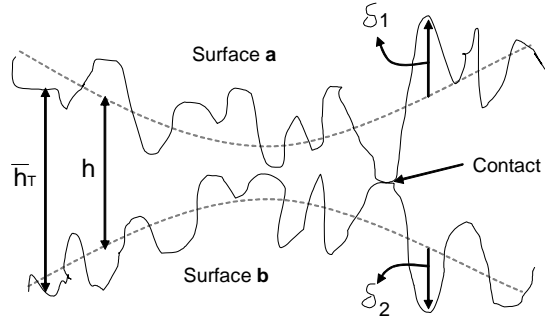


Figure 1: The geometry for average film-gap \bar{h}_T

where, the normal probability density function $f(\delta)$ for a Gaussian distribution is defined as-

$$f(\delta) = \frac{1}{\bar{\sigma} \sqrt{2\pi}} \exp \left(-\frac{\delta^2}{2\bar{\sigma}^2} \right) \quad (6)$$

From equations (5) and (6), the average film-gap in dimensionless form is rewritten as-

$$\bar{H}_T = \frac{H}{2} \left[1 + \operatorname{erf} \left(\frac{H}{\sqrt{2}\sigma} \right) \right] + \frac{\sigma}{\sqrt{2\pi}} \exp \left(-\frac{H^2}{2\sigma^2} \right) \quad (7)$$

For infinite line contact of cylindrical solids, $h_g(x)$ may be expressed by a parabolic approximation as $h_g(x) = \frac{x^2}{2R_x}$, thus, the film shape in the dimensionless form at any point X_i is given by

$$H(X_i) = H_0 + \frac{X_i^2}{2} - \frac{1}{\pi} \int_{X_{in}}^{X_{out}} [P(X') + P_c(X')] \ln |X - X'| dX' \quad (13)$$

H_0 contains the constant term of $H_d(X)$.

The density-pressure relation given by Dowson and Higginson [16] with a linear thermal correction included in [17, 18] is adopted in this paper in dimensionless form-

$$\rho_i = \left[1 + \frac{0.6 \times 10^{-9} p_H P_i}{1 + 1.7 \times 10^{-9} p_H P_i} \right] \times (1 - \beta T_0 \theta_i) \quad (14)$$

The dimensionless form of the viscosity-pressure-temperature relation proposed by Roelands et al. [19] is employed here-

$$\eta_i = \exp\{[\ln \eta_0 + 9.67][-1 + (1 + 5.1 \times 10^{-9} p_H P_i)^Z] - \Gamma T_0 \theta_i\} \quad (15)$$

where, $Z = \frac{\alpha}{(\ln \eta_0 + 9.67)(5.1 \times 10^{-9})}$ The dimensionless load-carrying capacity W_T is determined by the following expression -

$$W_T = \frac{p_H b}{E R_x} \int_{X_{in}}^{X_{out}} [P + P_c] dX \quad (16)$$

In the numerical problem the applied load on the surfaces is assumed to be a constant. The dimensionless load balance equation for line contact problem can be written as:

$$\int_{X_{in}}^{X_{out}} [P + P_c] dX = \frac{\pi}{2} \quad (17)$$

The dimensionless mean unit flow in the X direction is defined as

$$Q_i = \rho_i \frac{8W_T}{\pi} \left[\bar{H}_T(i) - \phi_x(i) \frac{4W_T^2}{3\pi^2} \frac{H_i^3}{\eta_i U} \frac{(P_{i+1} - P_{i-1})}{2\Delta X_i} \right] \quad (18)$$

The temperature distribution within the lubricant film is calculated from the energy equation associated with the appropriate boundary conditions. The energy equation for infinite line contact problems, neglecting heat convection across the film and conduction along the film, can be expressed as

$$\frac{\partial}{\partial y} \left(k \frac{\partial T}{\partial y} \right) = \bar{\rho} c_p u \frac{\partial T}{\partial x} - T \beta u \frac{\partial p}{\partial x} - \bar{\eta} \left(\frac{\partial u}{\partial y} \right)^2 \quad (19)$$

where

$$u = -y \left(\frac{h-y}{2\bar{\eta}} \right) \frac{\partial p}{\partial x} + u_b \left(\frac{h-y}{h} \right) + u_a \frac{y}{h}$$

A parabolic temperature profile across the film used by Salehizadeh and Saka [20] which is given below, is employed to reduce the energy equation to a one dimensional form :

$$T(x, y) = (3T_a + 3T_b - 6T_m) \left(\frac{y}{h} \right)^2 + (6T_m - 2T_a - 4T_b) \frac{y}{h} + T_b \quad (20)$$

where

$$T_a = T(x, h), \quad T_b = T(x, 0), \quad T_m = \frac{1}{h} \int_0^h T(x, y) dy \quad (21)$$

The moving surface temperature obtained by Carslaw and Jaeger [21] can be written as

$$T_a = T_0 + \frac{k}{\sqrt{\pi \rho_a c_a k_a u_a}} \int_{x_{in}}^x \left(-\frac{\partial T}{\partial y} \right)_{[x=x', y=h]} \times \frac{1}{\sqrt{x-x'}} dx' \quad (22)$$

$$T_b = T_0 + \frac{k}{\sqrt{\pi \rho_b c_b k_b u_b}} \int_{x_{in}}^x \left(\frac{\partial T}{\partial y} \right)_{[x=x', y=0]} \times \frac{1}{\sqrt{x-x'}} dx' \quad (23)$$

3 Solution Technique

The Reynolds, elasticity and energy equations are solved simultaneously using a modified Houpert and Hamrock fast approach, which involves the following computational steps:

- (a) The solution of elasticity equation by the algorithm developed by Venner *et al.* [22].
- (b) The simultaneous solution of thermal Reynolds equation and load balance equation by Newton-Raphson method.
- (c) The solution of surface temperature equations by Venner *et al.* [22].
- (d) The solution of energy equation by Newton-Raphson iterative scheme.

The standard central difference scheme is used to approximate the Reynolds equation and the energy equation in the system. For a set of input parameters, the numerical solution is achieved by a pressure-temperature iteration between the Reynolds, elasticity, load balance, energy and surface temperature equations. In the present analysis, a standard hertzian pressure distribution is adopted as the initial pressure distribution. In most of the cases presented in this paper $X_{in}=-4.5$, $X_{out}=1.5$ and a uniform grid of 660 points is used for the whole domain. The common input data for the thermal solutions are shown in Table 1.

The convergence criteria used for the present study are given below:

Table 1: **Properties of lubricant and solid**

Property	Value
Coefficient of lubricant thermal expansivity, $\beta(K^{-1})$	6.4×10^{-4}
Inlet density of lubricant, $\rho_0(Kg/m^3)$	846
Inlet temperature of lubricant, $T_0(K)$	313
Inlet viscosity of lubricant, $\eta_0(Pas)$	0.04
Pressure-viscosity coefficient, $\alpha(Pa^{-1})$	1.59×10^{-8}
Specific heat of lubricant, $c_p(Jkg^{-1}K^{-1})$	2000
Thermal-viscosity coefficient of lubricant, $\Gamma(K^{-1})$	4.2×10^{-2}
Thermal conductivity of lubricant, $k(Wm^{-1}K^{-1})$	0.14
Equivalent radius of cylinders, $R_x(m)$	0.02
Thermal conductivity of rollers, $k_a, k_b(Wm^{-1}K^{-1})$	47
Specific heat of rollers, $c_a, c_b(Jkg^{-1}K^{-1})$	460
Density of solids, $\rho_a, \rho_b(Kgm^{-3})$	7850
Elastic modulus of solids, $E_{a,b}(Pa)$	2.0×10^{11}
Poisson's ratio of solids, $\nu(\text{dimensionless})$	0.3
Constant in force-compliance relationship (eq^n), k^*	0.003
Materials parameter, G	3500
Dimensionless total load, W_T	1.0×10^{-4}
Dimensionless speed, U	1.0×10^{-11}

1. For Pressure:

$$E_p = \frac{\sum_i |P_i^{n+1} - P_i^n|}{\sum_i P_i^{n+1}} < 1 \times 10^{-5} \quad (24)$$

2. For Temperature:

$$E_t = \frac{\sum_i |\theta_i^{n+1} - \theta_i^n|}{\sum_i \theta_i^{n+1}} < 1 \times 10^{-5} \quad (25)$$

where n denotes the number of iteration.

4 Results and Discussion

A numerical solution of the thermal EHL of infinite line contact rough surfaces using average flow model has been obtained. The contact surfaces are assumed to have the same surface structure and the same rms roughness. In all the calculations, the

total load W_T has been kept fixed and the central film thickness H_c is calculated .

The results are obtained in terms of surface roughness parameters which are: (1). surface pattern parameter γ and (2). hydrodynamic roughness parameter Λ . The surface pattern parameter γ is defined as the ratio of 0.5 correlation lengths of x and y profiles (i.e. $\gamma = \frac{\lambda_{0.5x}}{\lambda_{0.5y}}$). $\gamma < 1$, $\gamma = 1$ and $\gamma > 1$ correspond to transverse, isotropic and longitudinal surface pattern respectively.

The isotropic and transversely oriented roughness ($\gamma \leq 1$) restrict the pressure flow and consequently $\phi_x < 1$. Conversely, longitudinal surface roughness ($\gamma > 1$) enhances the pressure flow resulting $\phi_x > 1$. The hydrodynamic roughness parameter $\Lambda = H_c/\sigma$ characterizes the surface irregularities. A higher value of hydrodynamic roughness parameter Λ indicates a smaller asperity height implying a smoother surface. From the definitions of flow factor and average film-gap, ϕ_x tends to 1 and \bar{H}_T tends to H when σ tends to zero (Λ approaches infinity). In this case, the average Reynolds equation allowing the surface roughness by flow factors and average film-gap, reduces to the usual Reynolds equation for smooth surfaces. Generally, the data for $\Lambda = 6$ are considered to be equivalent solution for smooth surfaces with small error. In the present analysis, the results obtained for rough surfaces are compared with that of EHL for purely smooth surfaces. The difference of most sensitive characteristics of EHL such as temperature, central film thickness obtained for the rough surfaces for $\Lambda \geq 6$ with that of purely smooth surfaces is also reported. The present numerical problem is solved with the following set of parameters: $1/9 \leq \gamma \leq 9$, $1.5 \leq \Lambda \leq 10$, $0 \leq S \leq 1.9$, $W_T = 1.0 \times 10^{-4}$, $U = 1.0 \times 10^{-11}$ and $G = 3500$. The results obtained from the present study are compared with those reported by Hsu & Lee [23], Sadeghi & Sui [24] and Wang & Lin [8] as shown in Table 2, Table 3 and Table 4.

Table 2 shows a comparison of minimum film thickness obtained from the present method with that of Hsu & Lee [23] and Sadeghi & Sui [24]. It is seen that the present value is in a close agreement with that of [23, 24].

Table 2: Comparison of the minimum film thickness obtained from Hsu & Lee [23], Sadeghi & Sui [24] and the present study ($G = 3500$)

Dimensionless load, W	Dimensionless speed, U	%Slip S	Dimensionless minimum film thickness		
			Sadeghi	Hsu & Lee	present
1.3×10^{-4}	7.3×10^{-11}	10	0.1305	0.1201	0.1129
		20	0.1260	0.1156	0.1122
		30	0.1226	0.1119	0.1112

Table 3 compares the convergence of pressure spike, maximum film & surface temperatures, maximum difference in mass flow and computing time obtained from the

present method for smooth surfaces with that of Hsu & Lee [23]. It is seen from Table 3 that present results agree well with the results of [23].

Table 4 compares the mass flow rate obtained from the present study under isothermal EHL of rough surfaces with that of Wang & Lin [8] for $W_T = 1.0 \times 10^{-4}$, $U = 1.0 \times 10^{-11}$, $S = 0.0$, $G = 5000$, $T_a = T_b = T_m = 40^\circ C$. It is noticed from Table 4 that the mass flow rates obtained for rough surfaces from the present method are 6 – 14% lower than those obtained by Wang & Lin [8]. This is because the present study excludes the shear flow factor. However, the present values are in qualitative agreement with that of [8].

Table 3: Comparison of the present work with that of Hsu & Lee [23] for computing time, convergence of pressure spike, maximum mean film temperature $(T_m)_{max}$, maximum surface temperature of ‘roller b’ $(T_b)_{max}$ and the maximum mass flux defect [$U = 1.0 \times 10^{-10}$, $W = 1.0 \times 10^{-4}$, $S=1.0$, $G = 3500$]

Results obtained from	Pressure spike	$(T_m)_{max}$ ($^\circ C$)	$(T_b)_{max}$ ($^\circ C$)	Time (sec.)	mass flux defect(%)
Hsu & Lee	0.9460	155.30	90.90	938	0.1
present	0.9763	166.20	88.20	232	0.07

Table 4: Comparison of mass flow rate obtained from the present study under isothermal EHL of rough surfaces with that of Wang & Lin [8] [$W_T = 1.0 \times 10^{-4}$, $U = 1.0 \times 10^{-11}$, $S = 0.0$, $G = 5000$, $T_a = T_b = T_m = 40^\circ C$]

Λ	Mass Flow Rate $Q \times 10^5$					
	$\gamma = 1/6$		$\gamma = 1$		$\gamma = 6$	
	Wang & Lin	present	Wang & Lin	present	Wang & Lin	present
6	2.70	2.36	2.61	2.27	2.580	2.22
3	3.01	2.74	2.67	2.36	2.558	2.19
2	3.39	3.16	2.77	2.42	2.518	2.16

4.1 Effect of Surface Roughness Pattern Parameter on Pressure, Film Thickness, Mass Flow Rate and Temperature Profile

Figures 3-7 compare the film shape, pressure profile, mass flow rate, mean film and surface temperature distributions for smooth and rough surfaces under thermal consideration at various values of surface pattern parameter γ with hydrodynamic roughness parameter $\Lambda = 2$ and slide/roll ratio $S = 0.5$. Figure 3 shows the

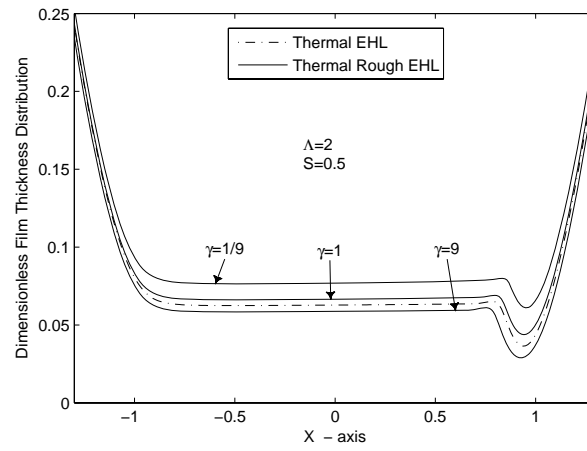


Figure 3: Dimensionless film-thickness distribution

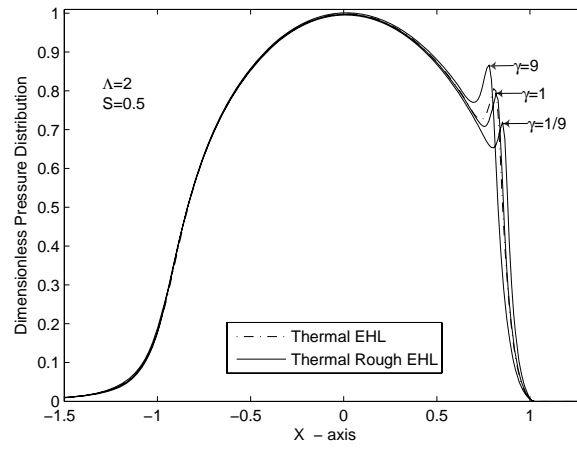


Figure 4: Dimensionless pressure distribution

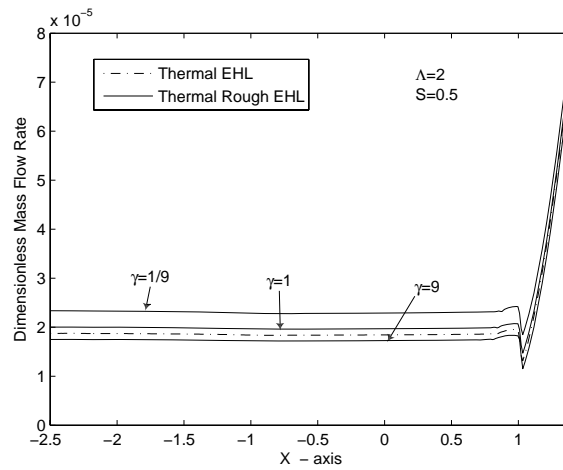


Figure 5: Dimensionless mass flow rate

comparison of film profiles between smooth and rough surfaces. It is seen that the film thickness for longitudinal surfaces has lower value than that of smooth surfaces whereas for isotropic and transverse surfaces the value is higher. The reason is that isotropic and transverse roughness restrict the mass flow in comparison to smooth surfaces, increasing the lubricant level. Conversely, longitudinal roughness offers less resistance to flow as compared to smooth surfaces, leading to a reduction in film thickness.

It is seen from figure 4 that the magnitude of the pressure spike for rough surfaces increases and the position shifts towards the center as the surface roughness pattern changes from transverse to isotropic to longitudinal. Among isotropic, transverse, longitudinal and smooth surfaces, the longitudinal roughness exhibits higher magnitude of pressure spike than that of smooth surfaces and seems to move closer to the center of the hertzian zone. This is so because longitudinally oriented surfaces have lower minimum film thickness than the smooth surfaces.

Figure 5 shows that the mass flow rate decreases significantly as the surface pattern parameter changes from $\gamma = 1/9$ to $\gamma = 9$. The transversely oriented surfaces have the highest value of mass flow rate, because, they have highest film thickness.

Figures 6 & 7 show the comparison of mean film and surface temperature distribution between smooth and rough surfaces.

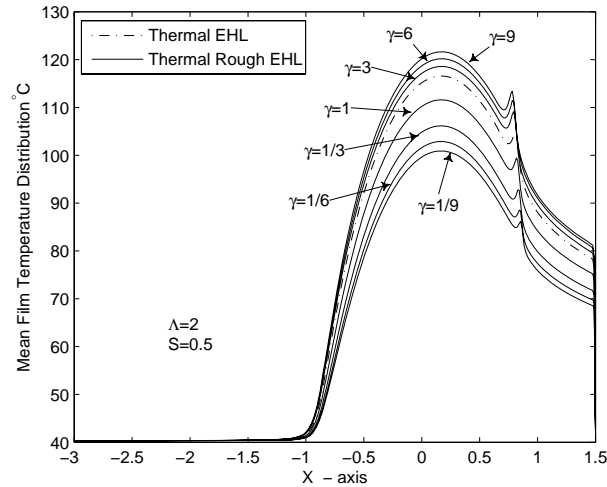


Figure 6: Mean film temperature distribution

The results obtained for rough surfaces indicate that the maximum mean film and surface temperature are increased as the surface pattern parameter changes from $\gamma = 1/9$ to $\gamma = 9$. The maximum mean film and surface temperatures for smooth surfaces play an intermediate role as longitudinal surfaces have greater temperature than that of smooth surfaces whereas isotropic and transversely oriented surfaces

have lower temperature. This is because, longitudinally oriented surfaces have highest contact load and least hydrodynamic load whereas isotropic and transversely oriented surfaces show a reverse trend and for smooth surfaces total load equals the hydrodynamic load.

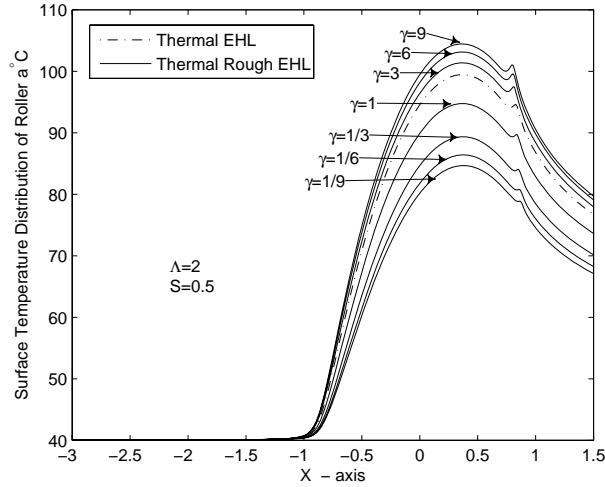


Figure 7: Surface temperature distribution of 'roller a'

Venner and Napel [25], Kumar et al [26] and Tonder and Jacobson [27] have investigated the effect of roughness on the EHL using deterministic models. They reported that the inclusion of surface roughness reduces the minimum film thickness and higher amplitude of surface roughness leads to higher pressure peaks. Sadeghi and Sui [9] from their thermal study with deterministic roughness model, added that film and surfaces temperatures are increased due to surface roughness.

The present study, which is the coupling of thermal effect with stochastic surface roughness, exhibits that for a fixed value of Λ and other parameters being same, the minimum film thickness, central film thickness and mass flow rate are reduced as surface pattern parameter γ increases from $1/9$ to 9 whereas, magnitude of pressure spike, maximum mean film temperature rise and maximum surface temperature rise are enhanced as γ increases. Among transverse ($\gamma < 1$), isotropic ($\gamma = 1$) and longitudinal ($\gamma > 1$) surface roughness, the transverse surface roughness ($\gamma = 1/9$) has highest film thickness, mass flow rate and hydrodynamic load whereas, lowest magnitude of pressure spike, mean film temperature, surface temperature and contact load. On the other hand, longitudinal surface roughness ($\gamma = 9$) shows a reverse trend. The results for smooth surfaces lie between ($\gamma \leq 1$) and ($\gamma > 1$).

4.2 Thermal EHL: Comparison Between Rough and Smooth Surfaces

It is obvious from the expressions for ϕ_x and \bar{H}_T that $\phi_x \rightarrow 1$ and $\bar{H}_T \rightarrow H$ when $\sigma \rightarrow 0$ (ie. $\Lambda \rightarrow \infty$, since $\Lambda = H_c/\sigma$ and $H_c \neq 0$).

Figure 8 shows the comparison of central film thickness H_c obtained for the rough surfaces with that of purely smooth surfaces.

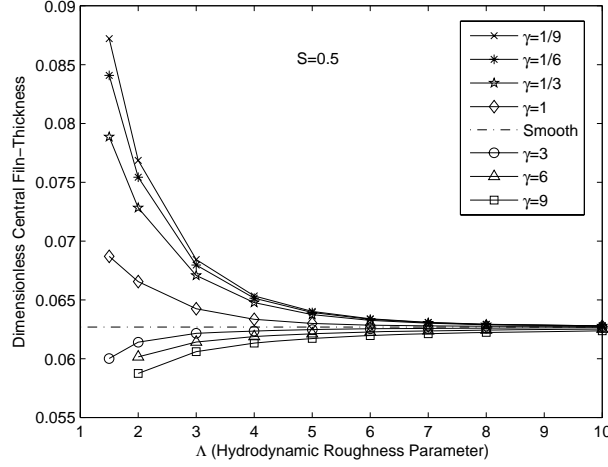


Figure 8: Comparison of central film thickness between rough and smooth surfaces

It is seen from figure 8 that for isotropic and transversely oriented surfaces ($\gamma \leq 1$), there is a decrease in central film thickness as Λ increases, whereas for a longitudinally oriented roughness ($\gamma > 1$) there is an increase in the film thickness with increasing Λ . This result is in line with those of [6, 8]. The reason is quite simple because the normally distributed isotropic and transversely oriented asperities restrict the mass flow. This causes an increase in the lubricant level in the lubrication region to maintain the continuity of flow giving rise to a larger central film thickness for this case. Further, as Λ increases, the relative magnitude of asperity height decreases and resistance of flow also decreases so lubricant level and thus the central film thickness decreases. On the other hand, longitudinally oriented surfaces offer less resistance to mass flow leading to a reduction in lubricant level resulting in a lower film thickness that increases with increasing Λ because total load is constant. It is interesting to see from figure 8 that the central film thickness for all surface patterns approaches to the central film thickness of purely smooth surfaces shown by dotted straight line as Λ increases from 6 to 10.

Table 5 clearly indicates that the central film thickness obtained for rough surfaces approaches to that of smooth surfaces as Λ increases from 6 to 10. Similar results are obtained for other EHL characteristics except temperature. Thus, it is

concluded that the results obtained for $\Lambda = 6$ can be considered as a nearly smooth surface solution with an absolute error around 1%.

Table 5: Percentage difference of central film thickness H_c obtained for thermal rough EHL for hydrodynamic roughness parameter $\Lambda \geq 6$ with that of thermal EHL of purely smooth surfaces. [$W_T = 1.0 \times 10^{-4}$, $U = 1.0 \times 10^{-11}$, $S = 0.5$, $G = 3500$]

Λ	% Error in H_c						
	$\gamma = 1/9$	$\gamma = 1/6$	$\gamma = 1/3$	$\gamma = 1$	$\gamma = 3$	$\gamma = 6$	$\gamma = 9$
6	+1.12	+1.04	+0.90	+0.25	-0.24	-0.67	-1.16
7	+0.62	+0.58	+0.51	+0.16	-0.18	-0.52	-0.91
8	+0.36	+0.34	+0.31	+0.11	-0.13	-0.41	-0.73
10	+0.16	+0.15	+0.14	+0.08	-0.07	-0.27	-0.50

Figure 9 illustrate the mean film temperature distributions for various surface roughness patterns with $S = 0.5$ and $\Lambda = 6$. The dotted curve represents mean film temperature obtained for purely smooth surfaces by neglecting surface asperities. It is observed that the maximum mean film temperature for rough surfaces is increased as surface patterns parameter γ changes from $1/9$ to 9 . A comparison of mean film temperature for rough and smooth surfaces reveals that longitudinal surfaces have higher temperature whereas isotropic and transverse surfaces have a lower temperature when compared with the results for smooth surfaces.

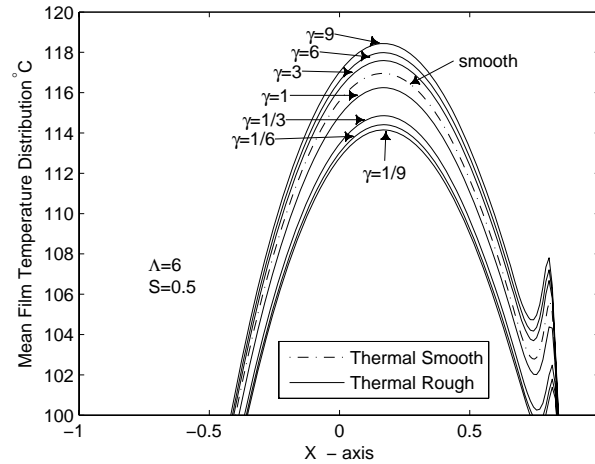


Figure 9: Comparison of maximum mean film temperature between smooth and rough surfaces

The percentage difference of maximum mean film temperature obtained for rough surfaces for $\Lambda \geq 6$ with that of smooth surfaces is reported in Table 6. It is noticed from Table 6 that the temperature results obtained for $\Lambda = 8$ may be considered as the nearly smooth solutions with an absolute error around 1%. Therefore, $\Lambda = 8$ can be considered to produce nearly smooth surface solution for thermal rough EHL problem with an absolute error around 1%.

Table 6: Percentage difference of maximum mean film temperature $(T_m)_{max}$ obtained for thermal rough EHL for hydrodynamic roughness parameter $\Lambda \geq 6$ with that of thermal EHL of purely smooth surfaces. [$W_T = 1.0 \times 10^{-4}$, $U = 1.0 \times 10^{-11}$, $S = 0.5$, $G = 3500$]

Λ	% Error in $(T_m)_{max}$						
	$\gamma = 1/9$	$\gamma = 1/6$	$\gamma = 1/3$	$\gamma = 1$	$\gamma = 3$	$\gamma = 6$	$\gamma = 9$
6	-2.39	-2.17	-1.79	-0.59	+0.54	+0.88	+1.27
7	-1.70	-1.53	-1.26	-0.33	+0.49	+0.76	+1.07
8	-1.19	-1.00	-0.88	-0.20	+0.45	+0.67	+0.93
10	-0.57	-0.50	-0.40	+0.05	+0.41	+0.56	+0.75

4.3 Effect of Hydrodynamic Roughness Parameter on Thermal EHL

Figures 10-17 show the relationship between the EHL parameters and the surface roughness parameters for slide/roll ratio $S = 1.0$.

It is observed from figure 10 that minimum film thickness for transverse ($\gamma = 1/9$, $\gamma = 1/6$, $\gamma = 1/3$) and isotropic ($\gamma = 1$) surface roughness patterns is a decreasing function of hydrodynamic roughness parameter Λ . However, for longitudinal surface patterns ($\gamma = 3$, $\gamma = 6$, $\gamma = 9$), it has increasing trend with increasing Λ . The physical reason is the same as in the case of central film thickness shown in figure 8.

Figure 11 shows the variation of the magnitude of pressure spike with respect to Λ for various surface roughness patterns. For longitudinal roughness, the magnitude of pressure spike decreases whereas for isotropically and transversely rough surfaces this exhibits an increasing trend with increasing Λ . The physical reasoning of this behavior lies in the inverse effect of minimum film thickness. The variation of mass flow rate shown in figure 12 follows the same trend as of minimum film thickness in figure 10.

Figures 13-15 show the surface roughness effect on the maximum mean film temperature rise, maximum surface temperature rise of faster moving 'roller a' and maximum surface temperature rise of slower moving 'roller b' respectively. It is seen that the maximum mean film temperature rise and maximum surface temperature

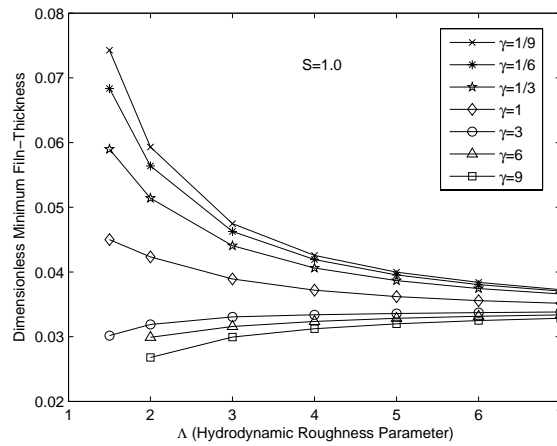


Figure 10: Effect of surface roughness on the minimum film thickness

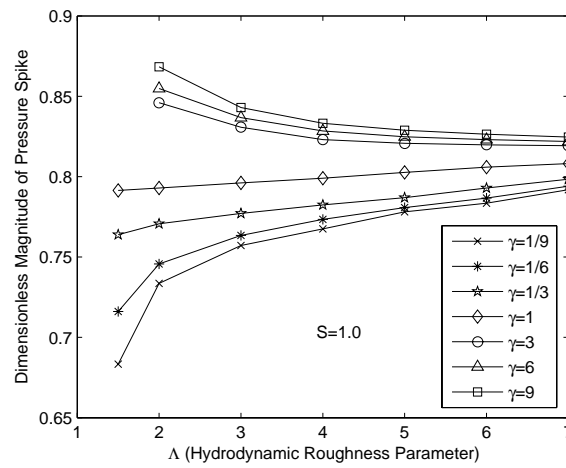


Figure 11: Effect of surface roughness on the pressure spike

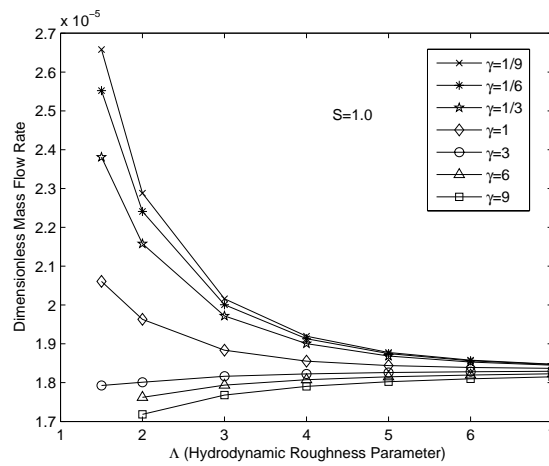


Figure 12: Effect of surface roughness on the mass flow rate

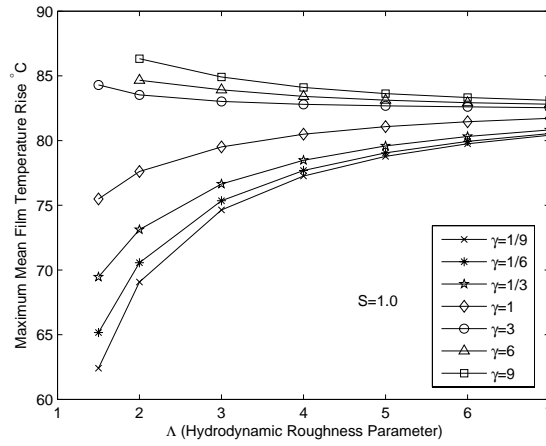


Figure 13: Effect of surface roughness on the maximum mean film temperature rise

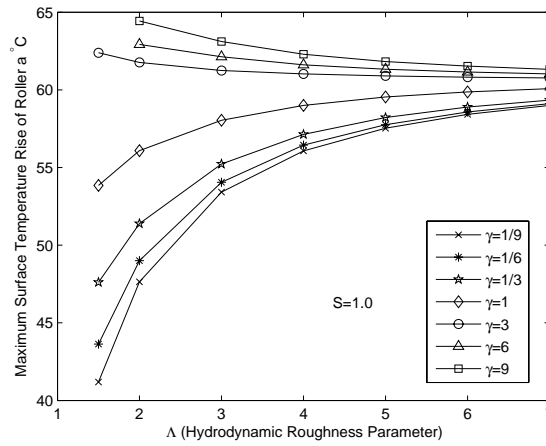


Figure 14: Effect of surface roughness on the maximum surface temperature rise of roller a

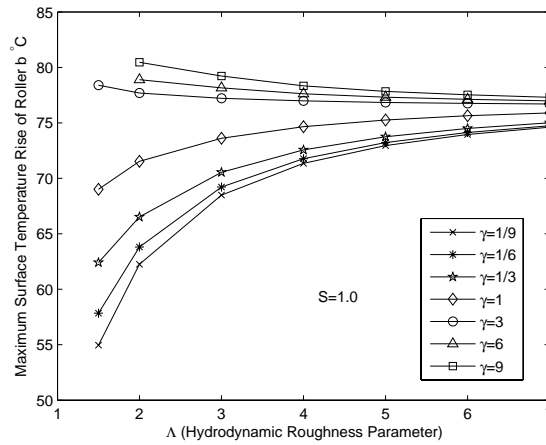


Figure 15: Effect of surface roughness on the maximum surface temperature rise of roller b

rise increase with increasing Λ for transverse surfaces ($\gamma = 1/9, \gamma = 1/6, \gamma = 1/3$) and isotropic surfaces ($\gamma = 1$). However, for longitudinal surface pattern ($\gamma = 3, \gamma = 6, \gamma = 9$), the maximum mean film temperature rise and maximum surface temperature rise exhibit decreasing trend. Further, it is seen that for a fixed value of Λ , the longitudinal surface roughness has highest film and surface temperature rise, whereas transverse roughness has least. This is because longitudinally oriented surfaces have highest contact load distributed over a large contact area giving rise to a larger temperature.

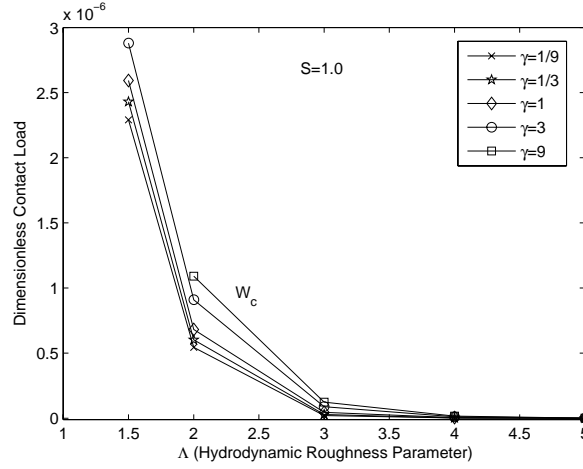


Figure 16: Effect of surface roughness on the contact load

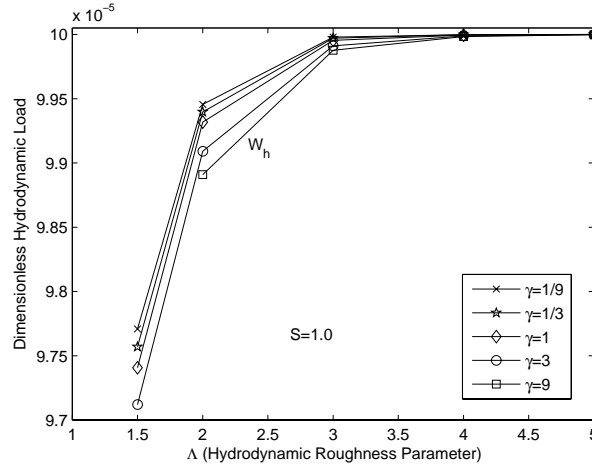


Figure 17: Effect of surface roughness on the hydrodynamic load

Figures 16 & 17 show the influence of surface roughness on the contact load W_c and the hydrodynamic load W_h respectively. It is observed that the hydrodynamic load W_h increases and consequently, the contact load W_c decreases with increasing

Λ for all surface roughness pattern having $\gamma = 1/9, 1/6, 1/3, 1, 3, 6, 9$. Further, it is seen that contact load W_c is maximum for longitudinally oriented surfaces ($\gamma = 9$) and decreases as γ decreases for a fixed value of Λ and same speed, slide/roll ratio, total load and material parameters, however, the ratio W_c/W_T is significant for $\Lambda \leq 3$. The reason of this behavior is that for longitudinally oriented surfaces, the central film thickness H_c is lowest, therefore for a fixed value of $\Lambda (= H_c/\sigma)$, relative magnitude of asperity height is higher than H_c , resulting in a higher contact load and consequently lower hydrodynamic load (\because total load W_T is fixed and $W_T = W_c + W_h$).

In the present study, combined thermal and roughness effects are investigated stating that for isotropic and transversely oriented surfaces ($\gamma \leq 1$), the minimum film thickness, central film thickness and mass flow rate are decreasing functions of Λ whereas, magnitude of pressure spike, maximum mean film temperature rise and maximum surface temperature rise are increased as Λ increases. The longitudinally oriented surfaces show reverse trend. Further, the contact load decreases and consequently hydrodynamic load increases as Λ increases for all patterns.

4.4 Isothermal and Thermal Rough EHL

Figure 18 compares the pressure and figure 19, the corresponding film thickness profiles between isothermal and thermal rough EHL for different surface roughness patterns: transverse surface ($\gamma = 1/9$), isotropic surface ($\gamma = 1$) and longitudinal surface pattern ($\gamma = 9$) for $\Lambda = 2$ & $S = 1.5$.

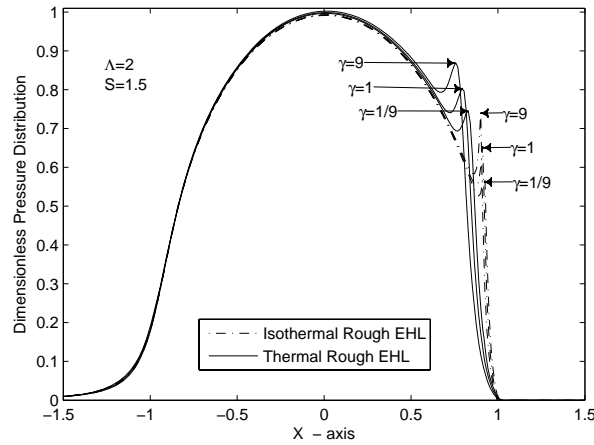


Figure 18: Dimensionless Pressure Distribution

It may be observed from figure 18 that for $\gamma = 1/9, 1$ & 9 the pressure exhibits a spike almost at the same location near the exit zone in case of isothermal rough

conditions. However, for the same parameters under thermal rough conditions, the magnitude of the pressure is increased and the spike seems to move closer to the center.

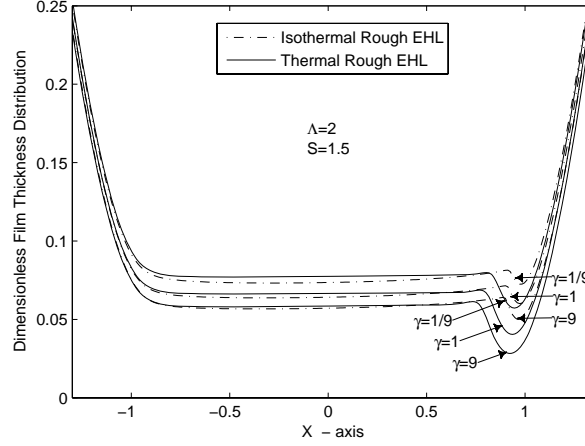


Figure 19: Dimensionless Film-Thickness Distribution

A significant reduction in the minimum film thickness due to thermal effect is seen from figure 19.

It is obvious from figures 18 & 19 that among these three surface roughness patterns, the longitudinal surface roughness causes the largest increment in the magnitude of pressure spikes and the greatest reduction in the minimum film thickness under both thermal and isothermal EHL.

The quantitative effect of surface roughness on isothermal and thermal EHL are summarized in Table 7 where the comparison of minimum film thickness H_{min} , magnitude of pressure spike P_s , mass flow rate Q , contact load W_c & hydrodynamic load W_h between isothermal and thermal conditions at various values of surface pattern parameters, are made for $\Lambda = 2$, $S = 1.5$.

It may be noted that the reduction in minimum film thickness for isothermal rough EHL is 17% as the surface pattern parameter changes from $\gamma = 1/9$ to $\gamma = 1$ and almost same when γ changes from 1 to 9. However, for the same parameters under thermal consideration the minimum film thickness shows a reduction of about 29% for the first change & about 30% for the second.

The increase in the magnitude of pressure spike when surface roughness pattern changes from transverse ($\gamma = 1/9$) to isotropic ($\gamma = 1$) is 14% for isothermal case and 8% for thermal; from isotropic surface ($\gamma = 1$) to longitudinal surface ($\gamma = 9$) the increment becomes 13% for isothermal case and about 8% for thermal case.

In the case of isothermal EHL, the reduction in mass flow rate is about 13% when γ changes from $1/9$ to 1 and about 11% from $\gamma = 1$ to $\gamma = 9$. However, an

Table 7: Comparison of the minimum film thickness H_{min} , magnitude of pressure spike P_s , mass flow rate Q , contact load W_c and the hydrodynamic load W_h between isothermal rough EHL and thermal rough EHL. [$W_T = 1.0 \times 10^{-4}$, $U = 1.0 \times 10^{-11}$, $S = 1.5$, $\Lambda = 2$, $G = 3500$]

Property	Rough-EHL	$\gamma = 1/9$	$\gamma = 1/3$	$\gamma = 1$	$\gamma = 3$	$\gamma = 9$
H_{min}	Isothermal	0.0724	0.0671	0.0600	0.0532	0.0499
	Thermal	0.0572	0.0492	0.0404	0.0309	0.0283
P_s	Isothermal	0.5741	0.6258	0.6542	0.7116	0.7414
	Thermal	0.7449	0.7833	0.8038	0.8462	0.8693
$Q \times 10^5$	Isothermal	2.2766	2.1627	1.9860	1.8447	1.7699
	Thermal	2.2799	2.1470	1.9504	1.7878	1.7076
$W_c \times 10^7$	Isothermal	4.1363	4.1621	4.1849	4.2665	4.3153
	Thermal	5.7308	6.4151	7.3119	9.5243	10.203
$W_h \times 10^5$	Isothermal	9.9586	9.9583	9.9581	9.9573	9.9568
	Thermal	9.9426	9.9358	9.9268	9.9047	9.8979

increase in mass flow rate, to the extent of about 15% when γ changes from 1/9 to 1 and about 13% from $\gamma = 1$ to $\gamma = 9$, has been observed due to the thermal consideration.

A less than 2% increase in contact load W_c from $\gamma = 1/9$ to $\gamma = 1$ and 3% from $\gamma = 1$ to $\gamma = 9$, has been observed under isothermal EHL. However, for thermal EHL, a significant increase in the contact load W_c extends to about 28% from $\gamma = 1/9$ to $\gamma = 1$ and about 40% from $\gamma = 1$ to $\gamma = 9$.

Hence, it is seen that thermal effect has significantly reduced the minimum film thickness, mass flow rate and hydrodynamic load whereas, it has significantly increased the magnitude of pressure spike, contact load, mean film temperature and surfaces temperatures.

5 Conclusion

A complete numerical solution to the problem of thermal-EHL of infinite line contact rough surfaces has been obtained. Both the surfaces are assumed to have same surface structure and the same rms surface roughness. The effects of surface roughness pattern, hydrodynamic roughness and thermal actions on EHL characteristics was investigated. The study yielded the following conclusions:

1. The inclusion of thermal effect has significantly influenced the bearing characteristics for rough EHL.

2. For a fixed value of Λ and other parameters being same, the minimum film thickness, central film thickness and mass flow rate are reduced as surface pattern parameter γ increases from 1/9 to 9 whereas, magnitude of pressure spike, maximum mean film temperature rise and maximum surface temperature rise are enhanced as γ increases. Thermal consideration enhances the effect of surface roughness on EHL characteristics.
3. The longitudinal surface roughness commonly causes the largest increment in the magnitude of pressure spikes and greatest reduction in the minimum film thickness under both thermal and isothermal EHL.
4. For $\Lambda = 2$, $S = 0.5$, an increase (about 5%) in the mean film and surface temperatures is observed due to longitudinal surface roughness ($\gamma = 9$) over that of smooth surfaces. On the other hand, a reduction (greater than 5%) in the mean film and surface temperatures is observed due to isotropic surface roughness ($\gamma = 1$) from that of smooth surfaces. Further, as the pattern changes from isotropic to transverse (from $\gamma = 1$ to $\gamma = 1/9$), there is an additional reduction in the temperature which is more than 15% from the value for the smooth surfaces.
5. The maximum mean film temperature rise and maximum surface temperature rise are increasing functions of Λ for transverse and isotropic surfaces ($\gamma \leq 1$), whereas decreasing for longitudinal surfaces ($\gamma > 1$).
6. The results obtained for $\Lambda = 8$ may be considered as a nearly smooth surface solution for thermal EHL problem with an absolute error around 1%.

List of Symbols

b	half Hertzian contact length, $4R_x\sqrt{W/2\pi}$ (m)
c_a, c_b	specific heat of roller a and b (J/kg-K)
c_p	specific heat of lubricant (J/kg-K)
$D_{i,j}$	discretized kernel
E	equivalent Young's modulus (Pa) $2/E = [(1 - \nu_a^2)/E_a + (1 - \nu_b^2)/E_b]$
E_p	error in pressure (eq^n24)
E_t	error in temperature (eq^n25)
G	dimensionless material parameter, αE
h	film thickness (m)
h_0	film constant (m)
h_c	central film thickness (m)
h_d	elastic deformation (m)

h_g	separation of surfaces in their undeformed state (m)
H	dimensionless film thickness, hR_x/b^2
H_0	dimensionless constant
H_c	dimensionless central film thickness, h_cR_x/b^2
H_e	dimensionless film thickness where $dP/dX = 0$
\bar{H}_T	dimensionless film-gap, \bar{h}_TR_x/b^2
k	thermal conductivity of lubricant ($Wm^{-1}K^{-1}$)
k_a, k_b	thermal conductivity of rollers ($Wm^{-1}K^{-1}$)
k^*	constant in force-compliance relationship (eq^n 9)
M	number of grid points used in the system
n	number of iteration
p	pressure (Pa)
p_c	contact pressure (Pa)
p_H	maximum Hertzian pressure, $Eb/4R_x$ (Pa)
P	dimensionless pressure, p/p_H
P_c	dimensionless contact pressure, p_c/p_H
Q_i	mean unit flow in the X direction
R_x	equivalent radius of cylinder (m)
S	slide/roll ratio, u_d/u_m
T_0	inlet lubricant temperature (K)
T_a, T_b	surface temperature of the rollers 'a' and 'b' (K)
T_m	mean temperature of lubricant film (K)
u_a, u_b	velocity of the roller a and b (m/sec)
u_d	sliding velocity, $u_a - u_b$ (m/sec)
u_m	average rolling velocity, $(u_a + u_b)/2$ (m/sec)
u	lubricant velocity (m/sec)
U	dimensionless speed parameter, $\eta_0 u_m / ER_x$
w	load per unit length (N/m)
W	dimensionless load, w/ER_x
W_c	dimensionless contact load, w_c/ER_x
W_h	dimensionless hydrodynamic load, w_h/ER_x
W_T	dimensionless total load, $W_T = W_c + W_h$
X	dimensionless coordinate, $X = x/b$
x	coordinate (m)
Z	Roelands pressure-viscosity parameter
α	pressure-viscosity coefficient (Pa^{-1})
β^*	mean radius of curvature of asperities
β	thermal expansivity of lubricant (K^{-1})
Γ	thermal-viscosity coefficient of lubricant (K^{-1})
γ	surface pattern parameter ($= \frac{\lambda_{0.5x}}{\lambda_{0.5y}}$)
$\lambda_{0.5x}$	0.5 correlation length of x profile
$\lambda_{0.5y}$	0.5 correlation length of y profile
δ_1, δ_2	random roughness amplitude of surfaces a and b
δ	combined roughness, $(\delta = \delta_1 + \delta_2)$
$\bar{\sigma}_1, \bar{\sigma}_2$	standard deviations of roughness heights δ_1 and δ_2
$\bar{\sigma}$	combined rms roughness, $(\bar{\sigma} = \sqrt{\bar{\sigma}_1^2 + \bar{\sigma}_2^2})$

σ	dimensionless combined rms roughness, $\bar{\sigma} R_x/b^2$
Λ	hydrodynamic roughness parameter, $(\Lambda = H_c/\sigma)$
Δ	distance between two neighboring grid points
η_0	inlet viscosity of lubricant (Pa s)
$\bar{\eta}$	viscosity of lubricant (Pa s)
η	dimensionless viscosity of lubricant, $\bar{\eta}/\eta_0$
θ	dimensionless mean temperature, $T_m/T_0 - 1$
ρ_0	inlet density of lubricant (Kg/m^3)
$\bar{\rho}$	density of lubricant (Kg/m^3)
ρ	dimensionless density of lubricant, $\bar{\rho}/\rho_0$
ρ_a, ρ_b	density of solid a and b (Kg/m^3)

References

- [1] S.J. Citron, Slow viscous flow between rotating concentric infinite cylinder with axial roughness, *ASME J. Appl. Mech.*, **29** (1962), 188 - 125.
- [2] H. Christensen and K. Tonder, The hydrodynamic lubrication of rough journal bearings, *Trans. ASME J. Lub. Tech*, **F** (1973) 166.
- [3] H.S. Cheng and A. Dyson, Elastohydrodynamic lubrication of circumferentially-ground rough disks, *ASLE Trans.*, **21** (1978), 25 - 40.
- [4] N. Patir and H.S. Cheng, An Average Flow Model for Determining Effects of Three Dimensional Roughness on Partial Hydrodynamic Lubrication, *Trans. ASME J. Lub. Tech*, **100** (1978), 12 - 17.
- [5] B.C. Majumdar and B.J. Hamrock, Effect of Surface Roughness on Elastohydrodynamic Line Contact, *Trans. ASME J. Lub. Tech*, **104** (1982), 401 - 409.
- [6] J. Prakash and H. Czichos, Influence of Surface Roughness and Its Orientation on Partial Elastohydrodynamic Lubrication of Rollers, *Trans. ASME J. Lub. Tech*, 105 (1983), 591 - 597.
- [7] T.A. Greenwood and T.H. Trip, The Contact of Two Nominally Flat Rough Surfaces, *Proc. Inst. Mech. Eng.*, **185** (1971), 625 - 633.
- [8] D.-S. Wang and J.-F. Lin, Effect of Surface Roupness on Elastohydrodynamic Lubrication of Line Contacts, *Tribology International*, **24** (1991), 51 - 62.
- [9] F. Sadeghi and P.C. Sui, Thermal Elastohydrodynamic Lubrication of Rough Surfaces, *ASME Journal of Tribol.*, **112** (1990), 341 - 347.
- [10] P. Kumar, S.C. Jain and S. Ray, Thermal EHL of Rough Rolling/Sliding Line Contacts Using a Mixture of Two Fluids at Dynamic Loads, *ASME Journal Of Tribol.*, **124** (2002), 709 - 715.

- [11] P. Kumar, S.C. Jain and S. Ray, Effect of Transverse Surface Roughness and Additives in TEHD contacts, *Tribology International*, **41** (2008), 502 - 514.
- [12] T. Almqvist, R. Larsson, Thermal Transient Rough EHL Line Contact Simulations by aid of Computational Fluid Dynamics, *Tribology International*, **41** (2008), 683 - 693.
- [13] N. Patir and H.S. Cheng, Application of Average Flow Model to Lubrication Between Rough Sliding Surfaces, *Trans. ASME J. Lub. Tech*, **101** (1979), 220 - 230.
- [14] M.K. Ghosh and B.J. Hamrock, Thermal Elastohydrodynamic Lubrication of Line Contacts, *Trans. ASLE*, **28** (1985), 159 - 171.
- [15] L.G. Houpert and B.J. Hamrock, Fast Approach for Calculating Film Thicknesses and Pressures in Elastohydrodynamically Lubricated Contacts at High Load, *Trans. ASME Journal of Tribology*, **108** (1986), 411 - 420.
- [16] D. Dowson and G.R. Higginson, *Elastohydrodynamic Lubrication*, Pergamon Press, (1966) Oxford
- [17] R.T. Lee and C.H. Hsu, A Fast Method for the Analysis of Thermal-Elastohydrodynamic Lubrication of Rolling/Sliding Line Contacts, *Wear*, **166** (1993), 107 - 117.
- [18] J. Bos, Frictional Heating of Tribological Contacts.” Ph.D. Thesis, University of Twente, Enchede (1994).
- [19] C.J.A. Roelands, J.C. Vlugter and H.I. Watermann, The Viscosity-Temperature-Pressure Relationship of Lubricating Oils and Its Correlation with Chemical Constitution, *ASME Journal Of Basic Enggineering*, **85** (1963), 601 - 610.
- [20] H. Salehizadeh and N. Saka, Thermal Non-Newtonian Elastohydrodynamic Lubrication of Rolling Line Contacts.” *ASME Journal Of Tribol.*, **113** (1991), 481 - 491.
- [21] H.S. Carslaw and J.C. Jaeger, *Conduction of Heat in Solids*, Oxford University Press, Oxford, U.K. (1959).
- [22] C.H. Venner, W.E. Ten Napel and R. Bosma, Advanced Multilevel Solution of the EHL Line Contact Problem, *ASME Journal of Tribol.*, **112** (1990), 426 - 432.
- [23] C.H. Hsu and R.T. Lee, An Efficient Algorithm for Thermal Elastohydrodynamic Lubrication Under Rolling/Sliding Line Contacts, *ASME J. Ttribol.*, **116** (1994), 762 - 769.

- [24] F. Sadeghi and P.C. Sui, Thermal Elastohydrodynamic Lubrication of Rolling/Sliding Line Contacts, *ASME Journal of Tribol.*, **112** (1990), 189 - 195.
- [25] C.H. Venner and W.E. Ten Napel, Surface roughness effects in an EHL Line Contact, *ASME Journal of Tribol.*, **114** (1992), 616 - 638.
- [26] P. Kumar, S.C. Jain and S. Ray, Study of Surface Roughness Effect in Elastohydrodynamic Lubrication of Rolling Line Contacts Using a Deterministic Model, *Tribology International*, **34** (2001), 713 - 722.
- [27] K. Tonder and J. Jakobson, Interferometric Studies of Effects of Surface Roughness on Lubricant Film Thickness Under Elastohydrodynamic Conditions, *ASME Journal Of Tribol.*, **114** (1992), 52 - 58.

Received: November, 2009